

1 **Evaluation of open and closed path sampling systems for determination**

2 **of emission rates of NH₃ and CH₄ with inverse dispersion modelling**

3 Yolanda Maria Lemes^a, Christoph Häni^b, Jesper Nørlem Kamp^a, Anders Feilberg^{*a}

4 ^aDepartment of Biological and Chemical Engineering, Aarhus University, Gustav Wieds Vej 10D, 8000 Aarhus,
5 Denmark.

6 ^bSchool of Agricultural, Forest and Food Sciences, Bern University of Applied Sciences, Länggasse 85, 3052
7 Zollikofen, Switzerland

8 **Corresponding author: email: af@bce.au.dk; Telephone: +45 30896099*

9 Declaration of interest: none

10 **Abstract**

11 The gas emission rates of ammonia (NH₃) and methane (CH₄) from an artificial source covering a surface
12 area of 254 m² were determined by inverse dispersion modelling (IDM) from point and line-integrated
13 concentration measurements with closed and open-path analyzers. Eight controlled release experiments
14 were conducted with different release rates ranging from 3.8 ± 0.21 to 17.4 ± 0.4 mg s⁻¹ and from $30.7 \pm$
15 1.4 to 142.8 ± 2.9 mg s⁻¹ for NH₃ and CH₄, respectively. The distance between the source and
16 concentration measurement positions ranged from 15 m to 60 m. Our study consisted of more than 200
17 fluxes averaged over intervals of 10 min or 15 min. The different releases cover a range of different
18 climate conditions: cold (< 5°C), temperate (< 13 °C) and warm (< 18 °C). As the average of all releases
19 with all instrument types, the CH₄ recovery rate Q_{BLS}/Q was 0.95 ± 0.08 (n = 19). There was much more
20 variation in the recovery of NH₃, with an average of 0.66 ± 0.15 (n = 10) for all the releases with the line-
21 integrated system. However, with an improved sampling line placed close to the source an average
22 recovery rate of 0.82 ± 0.05 (n = 3) was obtained for NH₃. Under comparable conditions, the recovery
23 rate obtained with an open-path analyzer was 0.91 ± 0.07 (n = 3). The effects of measurement distance,
24 physical properties of the sampling line, and deposition are discussed.

25 **Keywords:** Method validation, Ammonia, Methane, Inverse Dispersion Method, Backward Lagrangian
26 Stochastic, bLS

27 **1 Introduction**

28 The global agricultural system is currently facing one of its biggest humanitarian challenges:
29 feeding the world's rising population while preserving the environment and climate for future generations
30 (FAO, 2017). The agricultural sector is a major contributor to global greenhouse gas (GHG) emissions
31 (15%) and ammonia (NH₃) emissions (64%) (OECD and FAO, 2019), leading to air pollution, climate
32 change, deforestation, and loss of biodiversity (Aneja et al., 2009).

33 The European Union has established a reduction target for 2030 to reduce the GHG emissions by at
34 least 55% (EEA, 2019), compared to 1990, and NH₃ emissions by 19% (NEC Directive 2016/2284),
35 compared to 2005. Agriculture must contribute to GHG emission reductions, and valid estimates of GHG
36 emissions are important for national inventories regulation strategies and for selecting efficient mitigation
37 techniques.

38
39 Choosing the appropriate methodology to quantify gaseous emissions can be a challenge. In
40 particular agricultural sources are challenging as the sources often are small and inhomogeneous, exhibit
41 non-steady emissions over time (e.g. NH₃ emissions after slurry application (Hafner, 2018)) and are
42 influenced by other sources in close vicinity. Most of the methodologies have restrictions on the
43 measurement location and/or the source and involve complex instrumentation set-up (e.g., fast-response
44 analyzers, measurements at multiple heights). The micrometeorological mass balance (MMB) method
45 (Desjardins et al., 2004) requires measuring concentration at multiple positions several meters above the
46 ground, which is a challenge for obtaining high time resolution and it ignores the horizontal turbulent
47 transport (Hu et al., 2014). The tracer flux ratio method (TRM), which has also been used to measure
48 agricultural emissions (Vechi et al., 2022; Fredenslund et al., 2019; Delre et al., 2018), is a relatively
49 labor intensive and costly-intensive method typically with short intense measurement periods. In case of

50 dynamic emissions, this is not sufficient for resolving the temporal variations in emissions over days or
51 weeks.

52 The inverse dispersion method (IDM) based on backward Lagrangian Stochastic (bLS) dispersion
53 modelling (e.g. Flesch et al., 2004, 1995) has been widely used for the assessment of NH₃ and methane
54 (CH₄) emissions from many agricultural sources: dairy housing (Bühler et al., 2021; VanderZaag et al.,
55 2014; Harper et al., 2009), cattle feedlot (McGinn et al., 2019; Todd et al., 2011; van Haarlem et al.,
56 2008; Flesch et al., 2007; McGinn et al., 2007), application of liquid animal manure (Kamp et al., 2021;
57 Carozzi et al., 2013; Sintermann et al., 2011; Sanz et al., 2010), grazed pasture (McGinn et al., 2011;
58 Voglmeier et al., 2018), rice field (Yang et al., 2019), lagoon (Ro et al., 2014; Wilson et al., 2001),
59 composting stockpiles (Sommer et al., 2004), agricultural biodigester (Baldé et al., 2016b; Flesch et al.,
60 2011), farm (Flesch et al., 2005) and stored liquid manure (Lemes et al., 2022; Baldé et al., 2016a; Grant
61 et al., 2015; McGinn et al., 2008).

62 IDM has been tested in controlled release experiments with different conditions: ground level
63 source without obstacles (Flesch et al., 2014; McBain and Desjardins, 2005a; Flesch et al., 2004), ground
64 level source surrounded by a fence (Flesch et al., 2005; McBain and Desjardins, 2005a), elevated source
65 (Gao et al., 2008; McBain and Desjardins, 2005a), multiple emission sources (Hu et al., 2016; Ro et al.,
66 2011; Gao et al., 2008) and to quantify the effect of NH₃ deposition (Häni et al., 2018).

67 IDM is a function of the geometry and location of source and downwind concentration sensor
68 (including height for the sensor) and the turbulence characteristics in the surface layer. The statistical
69 properties of the flow in the atmospheric surface layer for the IDM are defined by the friction velocity
70 (u^*), roughness length (z_0), the Obukhov length (L), and wind direction (Flesch et al., 2004). Emissions
71 are derived from concentration measurements up- and downwind of the source, which could be
72 determined with point or line-integrated measurements from closed- or open-path analyzers. IDM
73 assumes an ideal atmospheric surface layer, which means i) a horizontally homogeneous and flat surface,

74 ii) homogeneity and quasi-stationarity with respect to the turbulence characteristics and iii) spatially
75 uniform emissions from a confined source (Flesch et al., 2004). Therefore, there should not be any
76 obstacles (e.g., trees, buildings) in close vicinity of the source to fulfil the required IDM assumptions.
77 Additionally, IDM has the limitation that there should not be any other sources of the same gas species
78 that affects up- and downwind concentration differently. The IDM is simple, flexible (Harper et al.,
79 2011), robust even in non-ideal conditions and has a reported accuracy of $100 \pm 10\%$ when it is properly
80 used (e.g., place of instruments, filtering criteria) (Harper et al., 2010). Moreover, IDM is a direct
81 measurement method that does not alter the physical properties of the source, and it is applicable for both
82 small and large emissions of any shape of sources (Flesch et al., 2004) as opposed to indirect enclosure
83 methods (e.g. chambers measurements).

84 Concentration measurements are mostly done with an open-path optical system (e.g. Baldé et al.,
85 2018; Bühler et al., 2021) because long path lengths (>50 m) enable a higher emission plume coverage
86 and avoids internal surfaces (e.g. tubes, pumps) where NH_3 can adsorb (Shah et al., 2006; Vaittinen et al.,
87 2014). However, open-path has a limitation on low concentration measurements (<10 ppb for CH_4 and
88 NH_3) (Bai et al., 2022) and requires complex calibrations to reduce the uncertainty of the measurements
89 (Häni et al., 2021; DeBruyn et al., 2020). In addition, it requires intensive labor to move and optically
90 align the instruments to different positions depending on the predominant wind direction. Commercially
91 available open-path analyzers exhibit limitations with respect to acceptable detection limits (Häni et al.,
92 2021). Closed-path analyzers have rarely been used together with the IDM (Ro et al., 2011) due to its
93 limitation caused by adsorption of NH_3 in the system. In addition, closed path analyzers have only been
94 used for point measurements, which challenges the ability to catch the emission plume and makes it
95 sensitive to wind direction accuracy.

96 Data filtering is needed to ensure accuracy of the IDM, which is related to the meteorological
97 conditions (e.g., wind speed, atmospheric stability) and wind direction. The quality criteria for filtering
98 are based on the atmospheric conditions in a measurement interval to ensure the assumptions of the model

99 is adequately meet, which also lower the uncertainty of the resulting data. Different criteria have been
100 used in previous studies: Flesch et al. (2005) recommend to remove data where $u^* < 0.15 \text{ m s}^{-1}$, $|L| < 10 \text{ m}$
101 and $z_0 > 1 \text{ m}$, whereas McBain and Desjardins, 2005 recommend $u^* < 0.19 \text{ m s}^{-1}$, $|L| \leq 3 \text{ m}$ and $z_0 > 1 \text{ m}$.
102 Flesch et al. (2014) suggest the filtering criteria for the night of $u^* < 0.05 \text{ m s}^{-1}$ and the gradient between
103 measured and MO-calculated temperature ($|\Delta\Delta T|_{\text{thres}} = 0.05 \text{ K}$). Bühler et al. (2021) removed data
104 where $u^* < 0.05 \text{ m s}^{-1}$, $|L| < 2 \text{ m}$, $z_0 > 0.1 \text{ m}$, standard deviation of the horizontal wind components (u, v)
105 divided by $u^*(\sigma_{u,v}/u^*) > 4.5$ and Kolmogorov constant ($C0 > 10$).

106 This study aimed to assess the applicability and performance of a closed-path analyzer used with a
107 sampling system that allows for line integrated concentration measurements used with the IDM for
108 determining emission rates of CH_4 and NH_3 . This novel measuring system will allow for measuring
109 emissions from sources with low emission rates and will have good flexibility for moving it around the
110 source depending on the wind direction in order to increase the probability of catching the emission
111 plume. This novel method is assessed by eight controlled releases of CH_4 and NH_3 combined with up- and
112 downwind measurements in different positions using point and line-average concentration provided with
113 closed- and open-path analyzers. The use of CH_4 and NH_3 and open- and closed-path systems to measure
114 concentration will give us an opportunity to: i) test the system of the line-average concentration
115 measurement with a closed-path analyzer; and ii) evaluate potential loss of NH_3 downwind from the
116 source by deposition and/or gas-to-particle conversion, processes that will not occur for inert CH_4 . This
117 controlled-release study is the first to compare the performances of open-path and line-integrated closed-
118 path systems for measuring emissions of NH_3 and CH_4 .

119

145 2 Material and methods

146 2.1 Site descriptions

147 From November 2019 to March 2022, eight controlled release experiments were performed at
148 different grassland sites under varying conditions (see [Table 1](#)). Five releases (I-DK to IV-DK and
149 VIII-DK) took place at AU campus Viborg, Denmark on two different fields (56°29'34.5"N / 9°34'28.3"E
150 and 56°29'36.4"N / 9°34'15.9"E). Three releases (V-CH to VII-CH) were performed at Bern University of
151 Applied Sciences, Switzerland (46°59'35.1"N / 7°27'43.1"E). At all sites, the terrain was horizontally flat,
152 and the height of the canopy varied between 15 and 25 cm for the different experiments. Obstacles upwind
153 of the artificial source were more than 100 m away in all experiments. There were no significant sources
154 near the experiment sites.

155 2.2 Instrumentation

156 In this study, different models of cavity ring-down spectroscopy (CRDS) [analyzers](#) from Picarro
157 (Picarro Inc., Santa Clara, CA, USA) were used to measure up- and downwind NH₃ and CH₄ concentration
158 ([Table 1](#)). Model G2201-i and model G4301 measure CH₄ concentration, G2103 measures NH₃
159 concentration, and G2509 measures CH₄ and NH₃ simultaneously. The CRDS is a closed-path analyzer with
160 continuous absorption that measures concentrations at approximately 0.5 Hz. The CRDS analyzer consists
161 of a laser and an optical cavity chamber with highly reflective mirrors, which gives an effective path length
162 of several kilometers. The light is absorbed in the cavity, and the decay of light intensity is called the ring-
163 down time, which is directly related to the concentration of the specific compound. It has been frequently
164 used to study agricultural emissions (e.g., Kamp et al., 2021; Pedersen et al., 2020; Kamp et al., 2019;
165 Sintermann et al., 2011). [Calibration of these CRDS instruments are conducted using a certified standard
166 gas and a dilution system with NH₃ free air before each release. Mass flow controllers \(Bronkhorst EL
167 FLOW, Ruurlo, Netherlands\) were used to obtain a range of desired concentrations in all calibrations. The
168 standard gas contained 10±0.31 ppm NH₃ \(Air Liquide, Horsens, Denmark\) and 100±2 ppm CH₄ \(Air
169 Liquide, Horsens, Denmark\). Calibration showed high linearity of the instruments with R² = 1. The CRDS](#)

170 instruments used pairwise for upwind and downwind measurements agreed within $\pm 5\%$ and no correction
171 of the instruments were therefore done, see Figure S5 and Figure S6 in the Supplementary Information.

172 In experiments V-CH to VII-CH, the downwind CH_4 concentration was measured with three
173 GasFinder3 analyzers (GF3, Boreal Laser Inc., Edmonton Canada) and the downwind NH_3 concentration
174 with three miniDOAS instruments (Sintermann et al., 2016). The GF3 analyzer is an open-path tunable
175 diode laser device that measures line-integrated CH_4 concentrations over path lengths of 5 to 500 m (i.e.
176 single path length between sensor and retroreflector) with a temporal resolution of 0.3 to 1 Hz. The
177 retroreflectors used in the experiments were equipped with seven corner cubes, suitable for path lengths
178 around 50 m. The GasFinder devices have been widely used to measure emissions from different type of
179 agricultural sources with the IDM (Bühler et al., 2021; McGinn et al., 2019; VanderZaag et al., 2014; Harper
180 et al., 2010; Flesch et al., 2007). The performance of the GF3 instruments is discussed in detail by Häni et
181 al. (2021). The GF3 instrument were intercompared with the calibrated CRDS instrument by measuring
182 ambient concentrations over at least one day and corrected accordingly. The applied corrections were $c =$
183 $c_{GF} + 0.14$, $c = c_{GF} + 0.22$, $c = c_{GF} + 0.12$ for the GF3 placed 15 m, 30 m, and 60 m from the source,
184 respectively.

185 The miniDOAS instrument is an open-path device that measures NH_3 , NO and SO_2 in the UV region
186 between 190 and 230 nm based on the differential optical absorption spectroscopy (DOAS; Platt and Stutz,
187 2008) technique. It provides path-averaged concentrations for path lengths between 15 m and 50 m, with
188 around 10 to 20 scans per second averaged over 1 minute. Ammonia emissions from agricultural sources
189 (Kamp et al., 2021; Kupper et al., 2021; Voglmeier et al., 2018) and from an artificial source (Häni et al.,
190 2018) have been measured with miniDOAS analyzers. Further details on the instrument is given in
191 Sintermann et al. (2016). The miniDOAS instruments were intercompared with the calibrated CRDS
192 instrument by measuring ambient concentrations over at least one day. The miniDOAS offset concentration
193 from the reference period 08-10-2021 from 15:30 to 17:00 was added ($3.2 \mu\text{g m}^{-3}$), whereas no correction
194 of the slop/span was necessary.

207

208 2.3 Gas release from an artificial source

209 The artificial source area had a gas distributor unit at the center and eight 1/4" polytetrafluoroethylene
210 (PTFE) tubes leave the distributor to get a circular shape of the source area. Each tube contained three
211 critical orifices (100 μm diameter, stainless steel, LenoxLaser, USA) in series with 3 m distance between
212 them. In total, the 24 orifices covered a circular area of 254 m^2 .

213 Gas was released from a gas cylinder and the flow was controlled with a mass flow controller (in
214 Denmark: Bronkhorst EL FLOW, Ruurlo, Netherlands; in Switzerland: red-y smart controller, Voegtlin
215 Instruments GmbH, Aesch, Switzerland). The source height, the content of the gas cylinders, and the release
216 rate for each experiment are given in [Table 1](#).

217

218

Formatted

219 **Table 1** Date, gas cylinders description, ammonia and methane release rate (RR), source and canopy height, downwind
 220 distance from source to instruments, type of system attached to the cavity ring-down spectroscopy (CRDS), and
 221 instrumentation of each controlled release experiment (CRE). G2103, G2202-i, G4301 and G2508 are different CRDS
 222 models, GF correspond to GasFinder and MD to miniDOAS.

| CRE | Date | Gas cylinder | | | NH ₃ RR | CH ₄ RR | Source height | Canopy height | Distance from source edge | System with CRDS | Instruments |
|---------|------------------------------------------------------------|---------------------------------------------------------------------|-------|-------|-----------------------|-----------------------|---------------|---------------|---------------------------|------------------------------------------------------------------------------------------------|--------------------------------------|
| | | Content | [bar] | total | [mg s ⁻¹] | [mg s ⁻¹] | [cm] | [cm] | [m] | | |
| I-DK | 29-11-2019 11:50 – 12:50 | 5% NH ₃ and 95% N ₂ ± 2%* | 62 | 1 | 4.6 ± 0.3 | - | 0 | 20 | 50 | Point 40°C | 2 G2103 |
| II-DK | 29-11-2019 14:00-14:30 | 99% CH ₄ and 1% N ₂ ± 2%* | 62 | 1 | - | 30.7 ± 1.4 | 0 | 20 | 50 | Point 40°C | G2201-i and G4301 |
| III-DK | 12-10-2020 11:45-15:15 | 5% NH ₃ and 95% CH ₄ ± 2%* | 62 | 1 | 3.8 ± 0.21 | 68.7 ± 3.7 | 0 | 25 | 35 - 60 | 16m line 40°C (Line 1) | G2103, G4301 and G2508 |
| IV-DK | 20-07-2021 10:30-16:00 | 10% NH ₃ and 90% CH ₄ ± 2%* | 62 | 2 | 17.4 ± 0.4 | 142.8 ± 2.9 | 50 | 18 | 15-30 | 12m line 40°C (Line 2) | G2103, G4301 and G2508 |
| V-CH | 09-10-2021 10:00-12:10 | 10% NH ₃ and 90% CH ₄ ± 2% ⁺ | 27 | 2 | 15.2 ± 0.3 | 128.9 ± 2.7 | 0 | 15 | 15 - 30 - 60 | 16m line 40°C (Line 1) | G4301, G2508, 3 GF and 3 MD |
| VI-CH | 09-10-2021 14:20-16:50 | 10% NH ₃ and 90% CH ₄ ± 2% ⁺ | 27 | 4 | 13.2 ± 0.3 | 111.8 ± 2.2 | 0 | 15 | 15 - 30 - 60 | 16m line 40°C (Line 1) | G4301, G2508, 3 GF and 3 MD |
| VII-CH | 09-10-2021 17:20-17:50 11-10-2021 15:10-16:20 | 10% NH ₃ and 90% CH ₄ ± 2% ⁺ | 27 | 4 | 13.2 ± 0.3 | 111.8 ± 2.2 | 50 | 15 | 15 - 30 - 60 | 16m line 40°C (Line 1) | G4301, G2508, 3 GF and 3 MD |
| VIII-DK | 22-04-2022 12:30-15:00 | 10% NH ₃ and 90% CH ₄ ± 2%* | 62 | 2 | 14.5 ± 0.3 | 118.9 ± 2.8 | 50 | 7 | 15 | 12m line 40°C (Line 2)and 12m line 80°C with heated inlets (Line 3) | 3 G2508 |

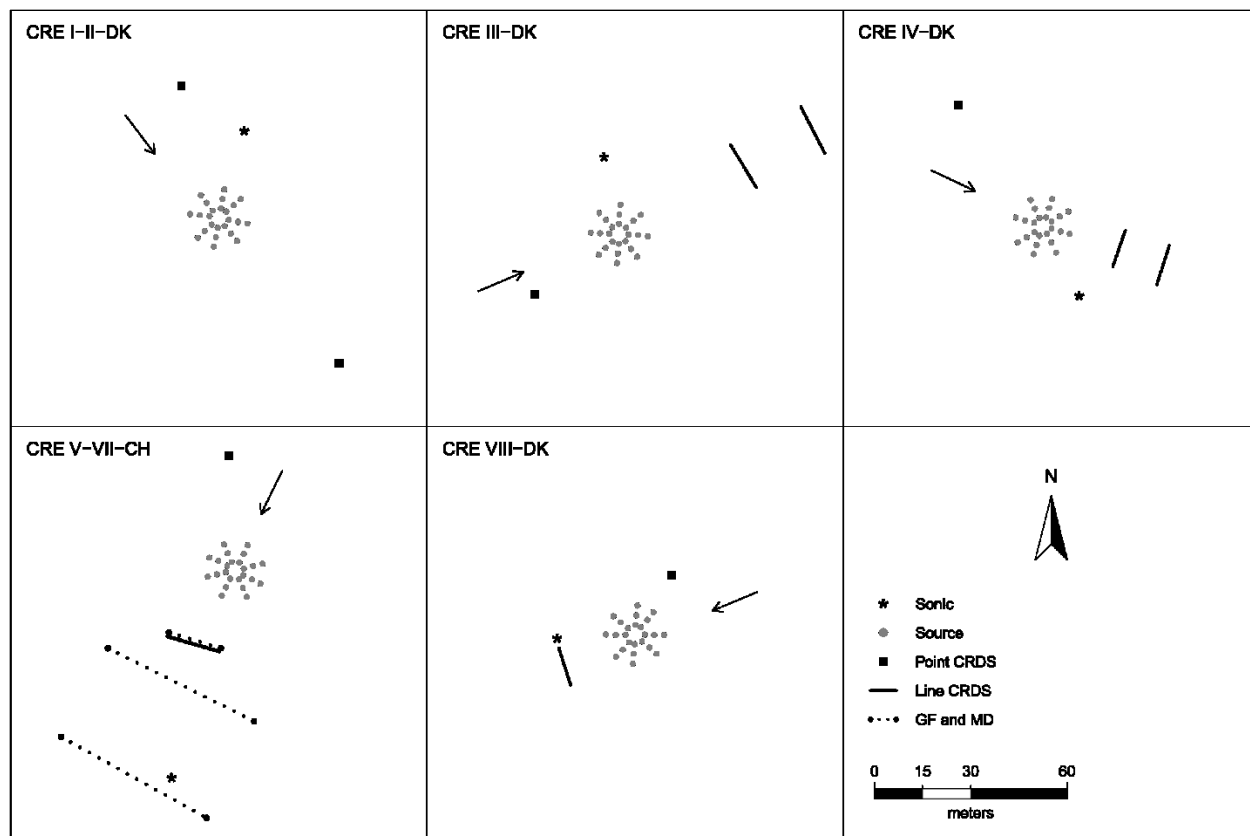
*Air Liquide, Horsens, Denmark
⁺Carbagas, Bern, Switzerland

249 2.4 Set-up

250 In the upwind position of all the experiments and in the downwind position of the I-DK and II-DK
251 experiment, the CRDS measured the concentration from a single point 1.5 m above ground through a
252 polytetrafluoroethylene (PTFE) tube that was insulated and heated to approximately 40°C. In the rest of the
253 experiments, the CRDS measured downwind concentration from a sampling line system of PTFE tubes
254 (Line 1 and Line 2) and polyvinylidene fluoride (PVDF) tube (Line 3) insulated and heated (40°C or 80°C).
255 The difference between the point and line-integrated system is the number of positions where the gas sample
256 is taken from. The point system had only one inlet, while the line-integrated had several. Three different
257 versions of the line-integrated system (line) were built and used during this research. In the III-DK, V-DK,
258 VI-CH, and VII-CH experiment, the sampling line system consisted of a 16 m tube with nine inlets, 2 m
259 between each inlet (Line 1). In the IV-DK and VIII-DK experiment, the sampling lines were 12 m long
260 with seven inlets, 2 m between each inlet (Line 2 and Line 3). The inlets are made of critical orifices (0.25
261 mm ID for I-DK to VII-CH and 0.5 mm ID for VIII-DK polyetheretherketone (PEEK)) that guarantee
262 uniform flow through each inlet (Line 1, Line 2 and Line 3). In the VIII-DK experiment, the sampling line
263 system including the inlets was heated to 80°C (Line 3).

264 Figure 1Figure 1 shows the position of the source area relative to the sampling position and the arrow
265 indicates the wind direction during the experiments. The downwind concentrations were measured in one,
266 two or three distance (Table 1Table 1). In the V-CH, VI-CH and VII-CH, downwind concentrations were
267 measured at the same time at 15 m, 30 m and 60 m distance from the edge of the source with multiple GF3
268 and miniDOAS instruments; one CRDS instrument was placed 15 m downwind (Figure 1Figure 1). The
269 distance between the reflector and the laser/detector of the GF3 and miniDOAS at the downwind position
270 parallel to the CRDS sampling line was also 16 m. For the other two downwind positions the path lengths
271 were 15 m and 50 m, respectively. The height of the measurement paths of all the open-path instruments
272 were between 1.2 and 1.5 m. The background concentration of NH₃ was stable with no sources in close
273 vicinity, thus in the three experiments, the average concentration of each instrument 10 min before the

274 release of each experiment was used as the NH₃ upwind concentration for the miniDOAS and the CRDS
 275 instruments. In the V-CH, VI-CH and VII-CH experiment, the measured NH₃ background concentration
 276 was 2.7 and 4.1 mg m⁻³, and 2.1 and 4.8 mg m⁻³ for the miniDOAS and the CRDS, respectively. The
 277 background concentration for V-CH and VI-CH was the same since they were carried out on the same day
 278 (see Table 1).



279
 280 *Figure 1 – Position of the orifices of the artificial source, ultrasonic anemometer (sonic), and the*
 281 *concentration analyzer used in the eight controlled release experiments (CRE) of this study. Three*
 282 *types of analyzers have been used: cavity ring-down spectrometer (CRDS), GasFinder (GF) and*
 283 *miniDOAS (MD). The arrow indicates the wind direction during each experiment.*

284 In Denmark, the three wind components were measured at 16 Hz with a 3D ultrasonic anemometer
 285 (WindMaster, Gill, Hampshire, UK) at 1.5 and 1.7 m height. In addition to concentration and wind, air
 286 temperature, and atmospheric pressure were also measured. In Switzerland, the wind components were
 287 measured at 20 Hz with a 3D ultrasonic anemometer (WindMaster, Gill, Hampshire, UK) at 2 m height.

288 Air temperature and atmospheric pressure were obtained from a meteorological station nearby the
289 experiment site.

290 A Global Positioning System (in Denmark: GPS Trimbel R10, Sunnyvale, California, USA; in
291 Switzerland: GPS Trimble Pro 6, Sunnyvale, California, USA) was used to record the position of all
292 instruments and the individual critical orifices of the source.

293 2.5 Inverse dispersion method

294 The measured gas emission rates (Q) from the artificial source were calculated in 15 min
295 (experiments conducted in Denmark) or 10 min average intervals (experiments conducted in Switzerland)
296 using the R (R Core Team, 2018) package bLSmodelR (<https://github.com/ChHaeni/bLSmodelR>;
297 version 4.3) as described by Häni et al. (2018). The simulation was performed with six million backward
298 trajectories (N) and the source area defined as 24 individual circles of 5 cm radius as described by Häni et
299 al. (2018) with a high performance computer cluster (PRIME - Programming Rig for Modern
300 Engineering, Aarhus University).

301 The emissions rate (Q) is proportional to the difference between measured concentration downwind
302 (C_{downwind}) from the source and the measured background concentration (C_{upwind}), and the dispersion
303 factor (D):

$$Q = \frac{C_{\text{downwind}} - C_{\text{upwind}}}{D} \quad (1)$$

304 The dispersion factor (D) is calculated as:

$$D = \frac{1}{N} \sum_{\text{TDinside}} \left| \frac{2}{w_{\text{TD}}} \right| \quad (2)$$

305 where N is the number of backward trajectories from the downwind analyzer location. The
306 summation refers to the trajectories touching inside the source area (TDinside) taking the vertical

307 velocity(w_{TD}) at touchdown into account. The calculation of D includes determination of wind profiles
308 and turbulence statistics that are based on the Monin-Obukhov Similarity Theory (MOST).

309 2.6 Surface deposition velocity

310 Ammonia is a relatively short lived gas in the atmosphere and can either be chemically converted, or
311 subjected to dry or wet deposition. Dry deposition of NH₃ is a complicated complex
312 phenomenon mechanism that is controlled restricted by both, both atmospheric dispersion towards, -and
313 land surface processes uptake at surfaces (thus, is correlated to several different conditions indicated by
314 e.g. wind speed, solar radiation, vegetation reactivity). The dry NH₃ deposition rate is usually often
315 expressed with a deposition velocity (v_d). ~~It is a complicated phenomenon that is controlled by both~~
316 ~~atmospheric and land surface processes (e.g. wind speed, solar radiation, vegetation reactivity).~~ In this
317 study, we assume model the dry deposition -as a canopy resistance ('big-leaf') approach where v_d takes
318 place uni-directionally and it is calculated with the canopy resistances (Hicks et al., 1987):

$$v_d = \frac{1}{R_a + R_b + R_c} \quad (3)$$

319 where R_a is the aerodynamic resistance, R_b is the quasi-laminar boundary resistance and R_c is the bulk
320 canopy resistance. Because R_a (is a function of wind speed and friction velocity) the resistance between the
321 concentration measurement height and the notional height z_0) (Baldocechi et al., 1987) that is already
322 included in the bLS model calculations, therefore Eq. 3 can be simplified asto represent a surface
323 deposition velocity:

$$v_d^* = \frac{1}{R_b + R_c} \quad (4)$$

324 For each model trajectory calculation, tThis apparent surface deposition velocity is acting on each
325 touchdown outside the emitting source to provide individual dry deposition fluxes F_d from prevailing
326 touchdown concentration C_{TD} as:

$$F_d = -v_d^* C_{TD} \quad (5)$$

327

328 And, This thus, reduces the modelled trajectory concentration at each touchdown outside the source by:

$$\Delta C_d = C_{TD} * \left(\exp \left(-\frac{2 * v_d^*}{w_{TD}} \right) - 1 \right) \quad (6)$$

329

330 We refer to Häni et al. (2018) for the derivation of the above equation and a thorough explanation of
 331 the implementation of the dry deposition algorithm in the bLS model.

332 In this study, According to Garland (1977), R_b can was be calculated according to Garland (1977),
 333 with Eq. 5 as a function of the roughness length (z_0), the friction velocity (u^*), the kinematic viscosity of
 334 air (ν) and the molecular diffusivity of NH_3 in air (δ_{NH_3}):

$$R_b = \frac{1.45 \left(\frac{z_0 u^*}{\nu} \right)^{0.24} \left(\frac{\nu}{\delta_{NH_3}} \right)^{0.8}}{u^*} \quad (7)$$

335 Regarding R_c , it is related to the chemical characteristics of the studied gas and the characteristics of
 336 the leaf (e.g. type, size). There are different models to calculate R_c . Due to the complexity and the
 337 uncertainty of the determination of the resistance, R_c was calculated following the same procedure as by
 338 Häni et al. (2018) with the bLS model. It was assumed that $Q_{bLS}/Q < 1$ was solely due to dry deposition.
 339 A similar approach is used here, where 12 values of R_c from 0 to 500 s m⁻¹ were tested in the bLS model
 340 that includes ammonia deposition to estimate the R_c giving $Q_{bLS}/Q = 1$ in all intervals. This was done with

341 linear interpolation between the two points closest to $Q/Q = 1$. Using this estimated R_c and the calculated
 342 R_b value for each interval, v_d^* was estimated for all intervals with all instruments. The v_d^* values are
 343 compared to previously reported values for NH_3 .

344 Another approach for calculating the R_c is with an empirical equation, which will be used for
 345 calculating values for v_d^* . These calculated values will be compared to the values obtained with the bLS
 346 model. It is assumed that R_c is unidirectional and equal to the sum of the stomatal resistance R_s and the
 347 cuticular resistance R_w , see Eq.6.

$$\frac{1}{R_c} = \frac{1}{R_s} + \frac{1}{R_w} \quad (86)$$

348 The stomatal resistance R_s is calculated with equation Eq.7 (Wesely, 2007):

$$R_s = R_{s(\min)} \left[1 + \left(\frac{200}{SR + 0.1} \right) \right]^2 \frac{400}{T_s(40 - T_s)} \quad (79)$$

349 where $R_{s(\min)}$ is minimum bulk canopy R_s for water vapour that is assumed to be equals to 250 s
 350 m^{-1} (Lynn and Carlson, 1990), SR is the solar radiation, and T_s is the soil temperature.

351 The cuticular resistance is calculated with Eq. 8 (Massad et al., 2010):

$$R_w = \frac{R_{w(\min)} e^{a(100-RH)} e^{0.15T}}{(LAI)^{0.5}} \quad (810)$$

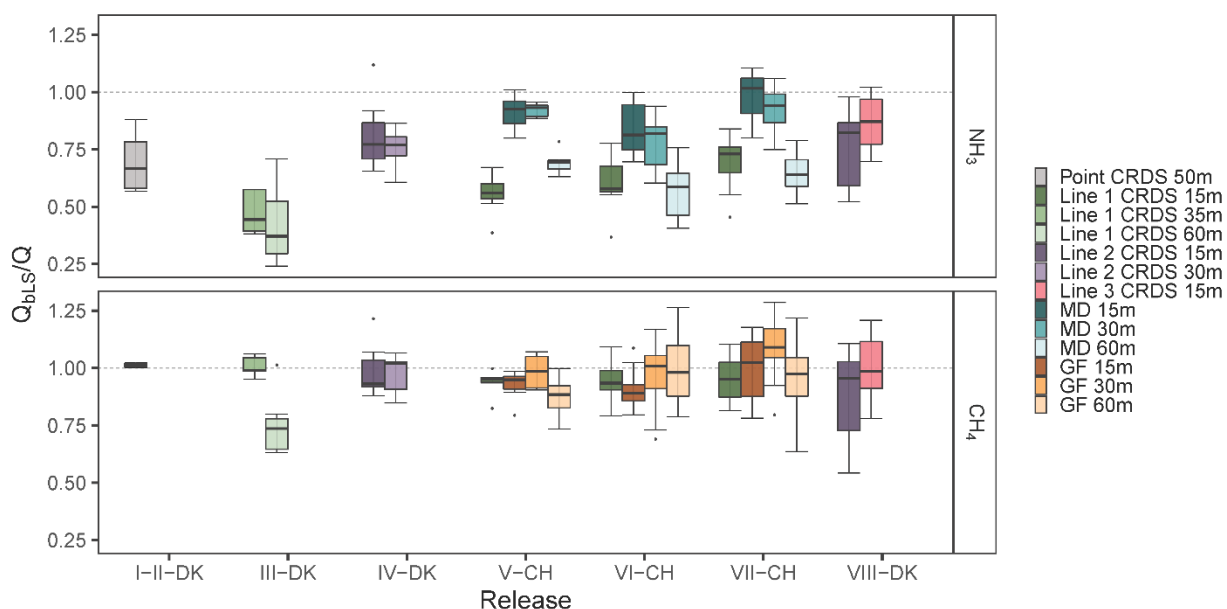
352 where $R_{w(\min)}$ is the minimum cuticular resistance, a is an empirical factor, RH is the relative
 353 humidity, T is the air temperature, and LAI is the leaf area index. The parameters $R_{w(\min)}$ (10 s m^{-1}), a
 354 (0.110) and LAI ($2 \text{ m}^2 \text{ m}^{-2}$) were obtained from Massad et al., 2010, Table 1.

388 3 Results and discussion

389 3.1 Recovered fractions of Ammonia and Methane

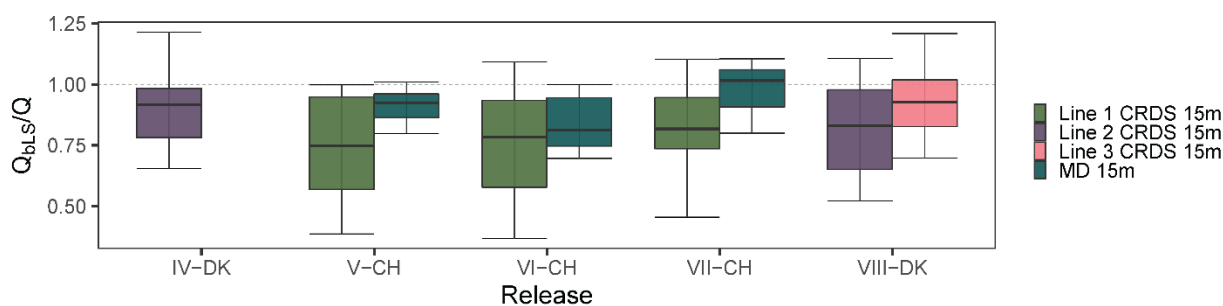
380 The accuracy of the bLS model is evaluated by the recovered NH_3 and CH_4 fractions, Q_{bLS}/Q , and
381 the standard deviation $\sigma_{Q_{\text{bLS}}/Q}$ for all the releases without taking NH_3 deposition into account. In all
382 experiments except I-DK and II-DK (Table 1), NH_3 and CH_4 were released simultaneously. The
383 use of these two gases give us the additional opportunity to assess potential loss of NH_3 downwind from
384 the source by deposition or gas-to-particle conversion, processes that will not occur for CH_4 due to its
385 inertness. As the average of all releases and measurement systems, the CH_4 recovery rate was 0.95 ± 0.08
386 ($n = 19$) (Figure 4). This recovery is similar to 0.93 ± 0.14 ($n = 8$) observed by Gao et al. (2008) with a
387 different controlled releases configuration and ground-level sources. There was more variation in the
388 recovery of NH_3 , with an average of 0.66 ± 0.15 ($n = 10$) for all the releases with the line-integrated
389 system. However, the improved sampling lines (Line 2 and 3) placed at 15 m downwind from the source
390 had an average recovery of 0.82 ± 0.05 ($n = 3$) for NH_3 (Figure 2). Under comparable conditions,
391 the NH_3 recovery rate obtained with the miniDOAS (MD) was 0.91 ± 0.07 ($n = 3$). Häni et al. (2018)
392 observed almost the same recovered fraction, 0.91 ± 0.12 , at 15 m from the edge of the source with the
393 MD. The recovery rates of all experiments in this study are shown in Figure 2, Figure 3 and
394 Figure 4, whereas climate conditions such as wind direction, friction velocity u_* , air temperature, relative
395 humidity (RH), soil temperature and solar radiation (SR) from each experiment are presented in
396 Supplementary information, Table S2. In addition, the average of the recovery fraction rates of
397 both gases and their relation in each release are shown in Table 2. I-DK and II-DK were conducted
398 during cold conditions ($\sim 5^\circ\text{C}$) with RH ranging from 65 % to 71 %, whereas IV-DK and VIII-DK were
399 conducted in warm conditions (14 – 18°C) with RH between 48 % and 63 %. The other releases were
400 conducted under moderate temperature conditions (10 – 13°C) with RH between 39% and 89%.

401 Additional information on the atmospheric conditions, weather conditions, and recovery fraction
 402 rates for each average time interval for each release are shown in Table S1 in the Supplementary
 403 Information.



404

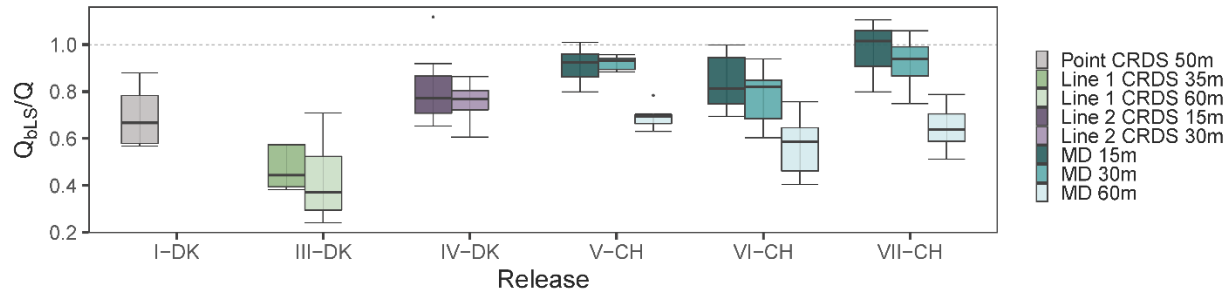
405



406

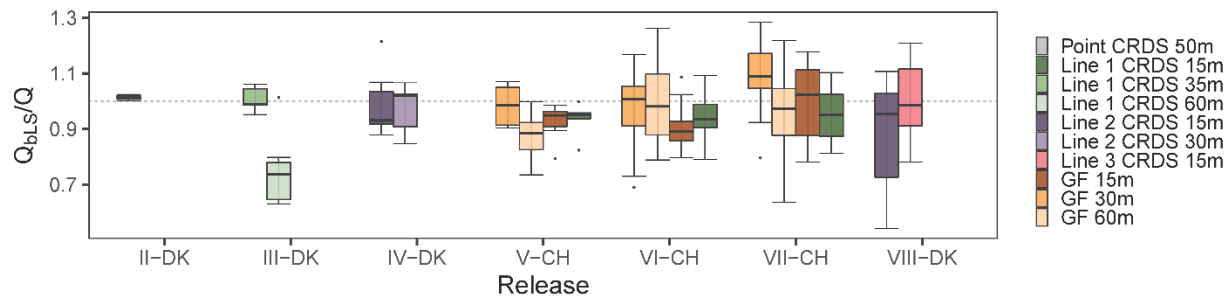
407 *Figure 2 .- The recovered fractions Q_{bLS}/Q of ammonia and methane from each the releases and analyzer.*
 408 *The downwind distance from the source to the analyzer is indicated in the legend, where line 1, 2 and 3,*
 409 *and miniDOAS (MD) are placed 15 m from the edge of the source. Line 1 had a length of 16 m, and it*
 410 *was heated to 40 °C. Line 2 had the same temperature as Line 1, but it was 12 m long. Line 3 had the*
 411 *same length as Line 2, but was heated to 80 °C. Error bars represent the standard deviation.*

412



413 *Figure 3. The recovered fractions Q_{bLS}/Q of ammonia from the releases where point concentration*
 414 *measurement was used and where concentration downwind distance was measured in two or three*
 415 *distances from the edge of the source. Line 1, Line 2 and Line 3 are described in the Figure 2 caption.*
 416

417



418 *Figure 4. The recovered fractions Q_{bLS}/Q of methane for each release and analyzer. The downwind*
 419 *distance from the source to the analyzer is indicated in the legend. Line 1, Line 2 and Line 3 are*
 420 *described in the Figure 2 caption.*
 421

422 Table 2 – Average of the recovery fractions Q_{bLS}/Q of ammonia and
 423 methane for each release and analyzer with standard deviation^{??}. Line 1,
 424 Line 2, and Line 3 are described in the Figure 2 caption.

| Release | Analyzer and distance | Q_{bLS}/Q_{NH3} | Q_{bLS}/Q_{CH4} | Q_{NH3}/Q_{CH4} |
|---------|-----------------------|-------------------|-------------------|-------------------|
| I-DK | Point CRDS 50m | <u>0.70±0.15</u> | | |
| II-DK | Point CRDS 50m | | <u>1.01±0.02</u> | |
| III-DK | Line 1 CRDS 35m | <u>0.47±0.09</u> | <u>1.01±0.05</u> | <u>0.47±0.21</u> |
| III-DK | Line 1 CRDS 60m | <u>0.42±0.17</u> | <u>0.75±0.13</u> | <u>0.57±0.44</u> |
| IV-DK | Line 2 CRDS 15m | <u>0.81±0.16</u> | <u>0.99±0.12</u> | <u>0.82±0.23</u> |
| IV-DK | Line 2 CRDS 30m | <u>0.76±0.08</u> | <u>0.97±0.08</u> | <u>0.78±0.14</u> |
| | Line 1 CRDS 15m | <u>0.53±0.11</u> | <u>0.92±0.07</u> | <u>0.57±0.23</u> |
| V-CH | MD, GF 15m | <u>0.90±0.08</u> | <u>0.91±0.08</u> | <u>0.99±0.13</u> |
| | MD, GF 30m | <u>0.91±0.05</u> | <u>0.98±0.07</u> | <u>0.92±0.09</u> |
| | MD, GF 60m | <u>0.68±0.05</u> | <u>0.80±0.23</u> | <u>0.86±0.30</u> |
| | Line 1 CRDS 15m | <u>0.60±0.10</u> | <u>0.95±0.09</u> | <u>0.63±0.20</u> |
| VI-CH | MD, GF 15m | <u>0.84±0.11</u> | <u>0.90±0.09</u> | <u>0.93±0.16</u> |
| | MD, GF 30m | <u>0.78±0.12</u> | <u>0.97±0.16</u> | <u>0.80±0.22</u> |

| | | | | |
|----------------|------------------------|------------------|------------------|------------------|
| | <u>MD, GF 60m</u> | <u>0.57±0.12</u> | <u>1.00±0.15</u> | <u>0.57±0.26</u> |
| | <u>Line 1 CRDS 15m</u> | <u>0.69±0.12</u> | <u>0.95±0.10</u> | <u>0.73±0.20</u> |
| <u>VII-CH</u> | <u>MD, GF 15m</u> | <u>0.98±0.10</u> | <u>0.99±0.15</u> | <u>0.99±0.18</u> |
| | <u>MD, GF 30m</u> | <u>0.92±0.10</u> | <u>1.08±0.15</u> | <u>0.85±0.17</u> |
| | <u>MD, GF 60m</u> | <u>0.64±0.09</u> | <u>0.95±0.18</u> | <u>0.68±0.23</u> |
| <u>VIII-DK</u> | <u>Line 2 CRDS 15m</u> | <u>0.77±0.17</u> | <u>0.89±0.20</u> | <u>0.86±0.31</u> |
| <u>VIII-DK</u> | <u>Line 3 CRDS 15m</u> | <u>0.87±0.11</u> | <u>1.00±0.14</u> | <u>0.86±0.19</u> |

441

442 **Table 3—Atmospheric and weather conditions in terms of friction velocity (u^*), wind speed (WS), air**
 443 **temperature (T_{air}), air pressure (P_{air}), soil temperature (T_{soil}), solar radiation (SR) and relative humidity (RH)**
 444 **during each release of this study.**

| Release | u^* [m s ⁻¹] | WS [m s ⁻¹] | T_{air} [°C] | P_{air} [hPa] | T_{soil} [°C] | SR [W m ⁻²] | RH [%] |
|---------|-------------------------------|----------------------------|--------------------------|---------------------------|---------------------------|----------------------------|-------------|
| I-DK | 0.23 ± 0.05 | 2.4 ± 0.5 | 4.5 ± 0.3 | 993.6 ± 0.3 | 5.5 ± 0.1 | 167.5 ± 34.4 | 69.6 ± 1.7 |
| II-DK | 0.19 ± 0.03 | 1.8 ± 0.1 | 4.8 ± 0.1 | 995.4 ± 0.1 | 5.6 ± 0.1 | 117.1 ± 8.4 | 64.7 ± 0.2 |
| III-DK | 0.22 ± 0.03 | 2.2 ± 0.3 | 11.7 ± 3.1 | 1005.3 ± 0.3 | 10.3 ± 0.2 | 139.5 ± 50.7 | 76.7 ± 1.3 |
| IV-DK | 0.45 ± 0.04 | 5.1 ± 0.5 | 17.9 ± 0.4 | 1009.1 ± 0.1 | 17.6 ± 0.2 | 378.8 ± 152.1 | 66.7 ± 2.4 |
| V-CH | 0.36 ± 0.03 | 4.5 ± 0.1 | 9.4 ± 0.3 | 958.9 ± 0.1 | 11.8 ± 0.0 | 238.3 ± 47.8 | 86.5 ± 1.7 |
| VI-CH | 0.20 ± 0.04 | 2.3 ± 0.4 | 11.1 ± 0.3 | 959.6 ± 0.0 | 12.7 ± 0.2 | 178.7 ± 41.4 | 75.5 ± 1.8 |
| VII-CH | 0.26 ± 0.08 | 3.2 ± 1.0 | 12.8 ± 0.9 | 959.4 ± 0.1 | 11.5 ± 0.9 | 340.8 ± 161.7 | 52.1 ± 13.2 |
| VIII-DK | 0.43 ± 0.05 | 4.7 ± 0.3 | 13.9 ± 0.6 | 1008.9 ± 0.2 | 8.7 ± 0.3 | 691.7 ± 53.2 | 51.4 ± 2.4 |

445

446 3.2 Sampling systems for closed-path measurement

447 Three different CRDS sampling line systems have been used from III-DK to VIII-DK. The difference
 448 between the lines was the length and the heating temperature. Line 1 had a length of 16 m, and it was heated
 449 to 40 °C. Line 2 had the same temperature as Line 1, but it was 12 m long. Line 3 had the same length as
 450 Line 2, but was heated to 80 °C, and the critical orifices have a higher inflow than Line 1 and Line 2 (see
 451 section 2.4 Set-up). We expect that decreasing the length and increasing the heating temperature of the line
 452 will improve Q_{bLS}/Q for NH_3 (no expected effect for CH_4) by avoiding adsorption and reducing the response
 453 time in the sampling line.

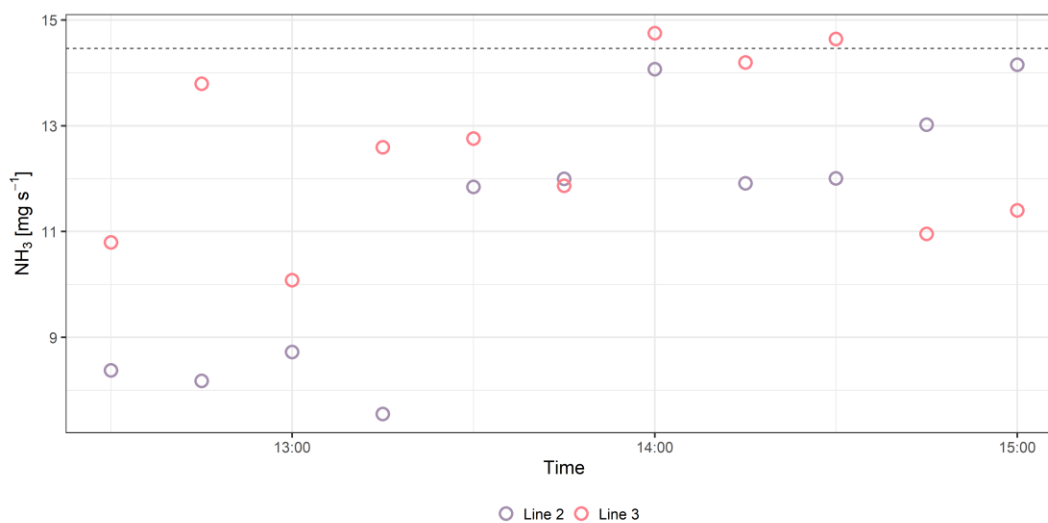
454 Line 1 was used with the source at ground level and elevated (Table 1), whereas the other
 455 two lines only with the source elevated. When the source was at ground level, Line 1 had a recovery rate
 456 ranging from 0.42 ± 0.17 to 0.60 ± 0.10 and from 0.75 ± 0.13 to 1.01 ± 0.05 for NH_3 and CH_4 , respectively.

482 The lowest and the highest NH₃ recovery rate of Line 1 are directly related to the furthest (60 m) and the
483 shortest (15 m) downwind distance measurement from the source. In addition, the standard deviation $\sigma_{Q_{bLS}/Q}$
484 at the furthest position is higher than at the closest position, which is in accordance with the results from
485 Häni et al. (2018). High uncertainty of the Q_{bLS}/Q is related to a smaller difference in concentration between
486 downwind and background concentrations and due to smaller D-values (Häni et al., 2018). This is also the
487 reason for the low CH₄ recovery rate of Line 1 in III-DK at 60 m (0.75 ± 0.13), downwind concentration is
488 only 4 – 10% higher than upwind concentrations since this is one of the lowest CH₄ releases rate ([Table
489 1](#)). This is in line with Coates et al. (2021), who observed that the bLS model underestimated 49%
490 of CO₂ released at 50 m fetch distance partially because the measured downwind concentration was close
491 to the background level. Therefore, in this study, the accuracy of Q_{bLS} is mainly influenced by the
492 uncertainty of the concentration measurement, hence the downwind distance is limited by the properties of
493 the gas analyzers and the size of the emission strength of the source. This means the system can be limited
494 in use if the emission source has a large height and low emission strength where, as a rule of thumb,
495 measurements should be conducted at a distance from the source at least 10 times the height of the source
496 (Harper et al., 2011).

497 In VII-CH, Line 1 was used with the source elevated and had a recovery rate of 0.69 ± 0.12 for NH₃
498 and 0.95 ± 0.10 for CH₄. Line 2 had a numerically higher recovery rate than Line 1, ranging from $0.76 \pm$
499 0.08 to 0.81 ± 0.16 and from 0.89 ± 0.20 to 0.99 ± 0.12 for NH₃ and CH₄, respectively in IV-DK and VIII-
500 DK. ~~As expected, the lowest NH₃ recovery rate of Line 2 was at the furthest downwind measurement
501 position (30 m).~~The length of the line appears to affect the NH₃ recovery rate; this might be due to the
502 increased surface area that NH₃ can adsorb to ~~stick~~, and there is a lower flow in each of the critical orifices
503 that decreases the response time of the system (Shah et al., 2006; Vaittinen et al., 2014). Looking at the
504 measured NH₃ rates over time ([Figure 3](#)~~Figure 5~~), higher emissions are reached with Line 3 for the first
505 hour indicating a faster time response compared to Line 2. However, after an hour there was not a clear
506 difference between the lines. The results indicate that increasing the sampling line temperature to 80 °C had

526 a positive effect on the recovery, which reached 87 % at a distance of 15 m. From the data obtained by the
 527 open-path analyzer (MD), we can conclude that deposition can cause a reduction in recovery in the order
 528 of 2-16% (Figure 2). Thus, the recovery obtained with the improved line (Line 3) approaches the
 529 recovery obtained with the open-path analyzer. It should be noted that a direct comparison between Line 3
 530 and the open-path analyzer (MD) has not been made and further improvement can still be suggested for the
 531 CRDS sampling line system. Specifically, increasing the flow through the sampling line and critical
 532 orifices will reduce NH₃ adsorption in the tubing material. However, similar flow rates through the
 533 can be achieved by increasing the flow through the tubing and the critical orifices but maintaining an even
 534 flow distribution through the discrete sampling orifices inlets in the sampling line must still be
 535 ensured.

536

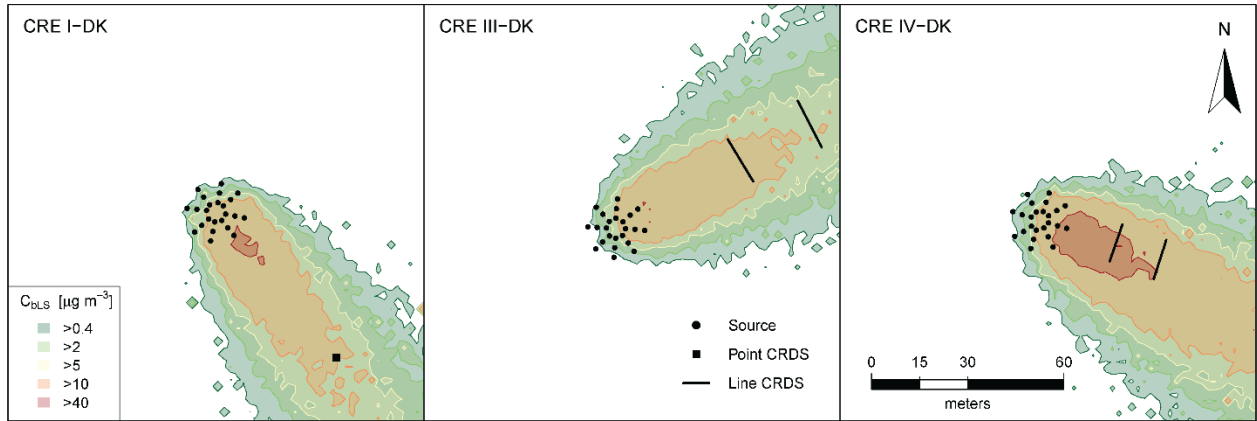


537

538 *Figure 35.- Ammonia (NH₃) fluxes measured with Line 2 and Line 3 in 10 min intervals average in VIII-*
 539 *DK.*

540 The point CRDS system had a recovery rate of 0.70 ± 0.22 and 1.01 ± 0.05 for NH₃ and CH₄,
 541 respectively. The benefit of the point CRDS system is mainly that increasing the flow in the tubing is less
 542 limited, since there are no critical orifices for which equal flow must be maintained. However, comparing
 543 point and line CRDS systems by the modelled concentration distribution (Figure 4), the line-
 544 integrated measurement system covers a larger part of the emission plume from the source in a higher

545 wind direction range. In addition, a line-integrated measurement system can reduce uncertainty in the
 546 IDM (Flesch et al., 2004), since it is less sensitive to error in the measured wind direction. This is in
 547 accordance with Ro et al. (2011), who observed an almost double recovery value of a line-integrated
 548 measurement system for CH₄ compared to a point measurement system using a photoacoustic gas
 549 monitor.



550

551 *Figure 46.- Contours of the modelled concentration distribution (C_{bLS}) for CRE I-DK, CRE III-DK and*
 552 *CRE IV-DK.*

553 3.3 Open-path measurement systems

554 The recovery rates for the GFs (CH₄) ranged from 0.87 ± 0.10 to 1.08 ± 0.15 . In V-CH to VII-CH,
 555 the corresponding standard deviation $\sigma_{Q_{bLS}/Q}$ of GF 15 m varies from 0.07 to 0.18, while Line 1 (placed
 556 parallel to GF 15 m) ranges from 0.06 to 0.10. These standard deviations $\sigma_{Q_{bLS}/Q}$ are comparable with
 557 those measured by Gao et al. (2009) (1.03 ± 0.16).

558 In V-CH and VI-CH (source at ground), the MDs (NH₃) had recovery rates ranging from $0.57 \pm$
 559 0.12 to 0.93 ± 0.03 . In VII-CH, MDs exhibit higher recoveries ranging from 0.64 ± 0.09 to 0.98 ± 0.10
 560 since the source was elevated. Generally, it is recommended to do a release experiment above ground
 561 level to reduce the probability of deposition close to the release area (McBain and Desjardins, 2005b). As
 562 expected, the recovery rate decreased with downwind distance of the sampling position due to NH₃
 563 deposition, which will be evaluated in section 3.4. Comparing MD at 15 m and Line 1 (placed in parallel)

586 in V-CH to VII-CH (~~Figure 2~~Figure 2), the recovery rates are higher for MD. The highest difference
587 between MD and Line 1 was in V-CH, where there were the highest RH (87%). However, there are no
588 clear patterns explaining the difference between emissions from the different measurement systems based
589 on atmospheric conditions (Supplementary information, Figure S2). Although, the improved recovery
590 with Line 2 (0.81 ± 0.16) and Line 3 (0.87 ± 0.11) in IV-DK and VIII-DK could be influenced by the
591 warmer conditions and solar radiation (Supplementary Information, Table S2Table 2), it is plausible that
592 the line improvements caused the increase. An increased flow through the orifices and higher temperature
593 of the sampling line will lead to less NH₃ adsorption thereby getting a better recovery from the release.

594 ~~These~~is results show the advantage of an open-path instrument compared to a closed-path
595 instrument to measure NH₃ emissions (~~Figure 2~~Figure 2), since open-path avoids prolonged response
596 caused by the adsorption of NH₃ to sampling materials (Shah et al., 2006; Vaitinen et al., 2014).

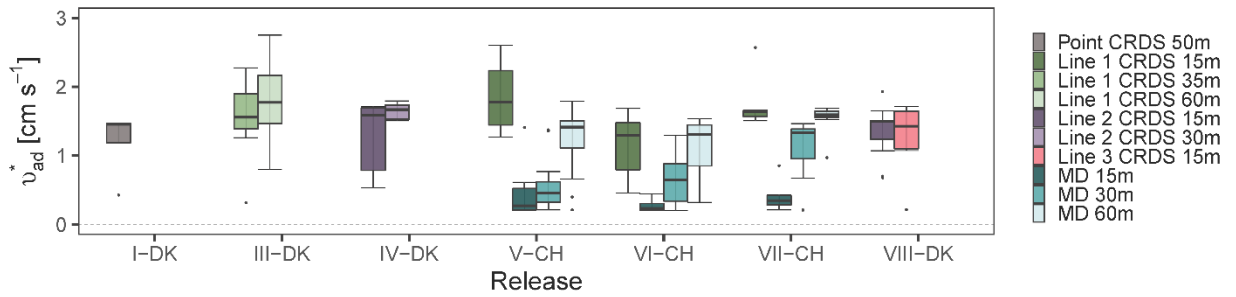
597 However, quality assuranceit is more ~~difficult to evaluate the quality of measurements by an~~ challenging
598 for open-path instruments ~~due to complexity~~because the use of a closed gas cell for calibration with a
599 certified gas standard is tedious and means that either ~~the instrument setup deviates significantly during~~
600 calibration compared to the ~~from field measurement~~of the calibration that depends on the path length
601 between the sensor and reflector (DeBruyn et al., 2020), ~~or the need~~ intercomparison to a reference
602 method (as an alternative to gas standard calibration) may also ~~instrument~~ introduces unknown
603 uncertaintiesof another instrument for intercomparison (Häni et al., 2021). In addition, the closed-path
604 system presented in this study (line CRDS) is more flexible with respect to moving the sampling line
605 around the source depending on the predominant wind direction. This ~~factor has different impact in~~ is
606 more particular important in areas with frequently ~~regularly~~ changing wind direction ~~different countries,~~
607 e.g. in the case in Denmark ~~wind direction change quite more often than in Switzerland.~~

632 3.4 Surface deposition velocity

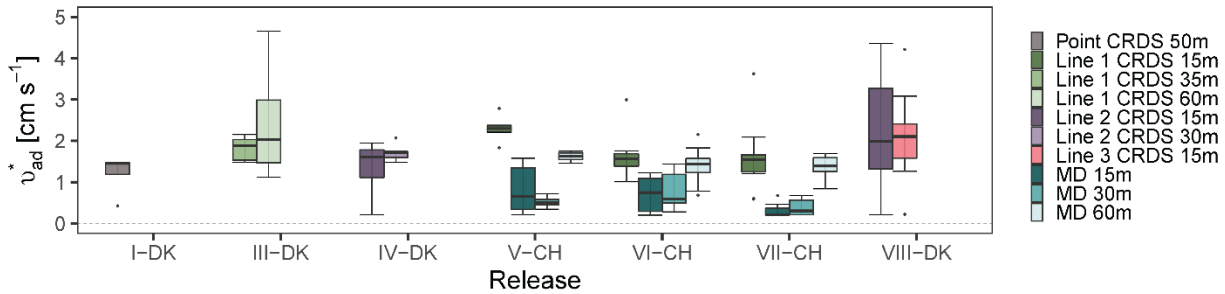
633 The corresponding surface deposition velocities (v_d^*) required to have a recovery rate $Q_{bLS}/Q =$
634 Q_{CH4} are presented in ~~Figure 5~~ Figure 7. This approach assumes ~~a complete a recovery equals to the~~
635 ~~measured Q_{CH4}~~ for each of the measurement systems when taking deposition into account, which is not
636 completely correct for closed-path sampling. In the following, therefore, we refer to deposition velocity
637 required to achieve $Q_{bLS}/Q = Q_{CH4}$ as the *apparent* deposition velocity (v_{ad}^*). This is included to provide
638 data on deposition velocities for ammonia for which data is currently very limited. The recovery rates
639 observed in Figure 2 show that the MD performed best, whereas lower Q_{bLS}/Q were seen in the sampling
640 lines, thus the lowest v_{ad}^* is expected from MD. Additional information of R_c and v_{ad}^* for each time
641 intervals in each experiment is shown in Table S1 in the Supplementary Information. The apparent
642 surface deposition velocities ranged from 0.2 to 12.82 cm s^{-1} for open-path data and from 0.2 to 4.27 cm s^{-1}
643 for the line sampling, ~~respectively~~. Häni et al. (2018) reported v_{ad}^* in the range from 0.3 to 1.1 cm s^{-1} . In
644 all the releases where downwind concentrations were measured at different positions, v_{ad}^* appears to
645 increase with distance ~~increases, with many cases~~. For example, in VI-CH, v_{ad}^* is 0.37 \pm 0.14, 0.78 \pm 0.4
646 and 1.14 \pm 0.54 cm s^{-1} at 15 m, 30 m and 60 m, respectively. The reason for this increase with distance is
647 presently unclear and should be investigated further. This is in line with the outcome of Asman and van
648 Jaarsveld. (1991); a significant fraction of the emitted NH_3 is deposited near the source, which supports
649 the regulations that do not allow livestock sources near sensitive eutrophic ecosystems (NEC Directive
650 2016/2284).

651 In V-CH, VI-CH and VII-CH, v_{ad}^* from Line 1 are 24.98, 42.23 and 45.31 times higher than MD at
652 15 m. As expected v_{ad}^* was higher for Line 1 as the Q/Q was lower for Line 1 compared to MD in these
653 experiments. Comparing the apparent deposition velocities from these experiments show comparable
654 values for Lines 2 and 3, but higher values for Line 1, i.e. Line 1 (VII-CH) had v_{ad}^* of 1.67 \pm 0.49,
655 whereas Line 2 and Line 3 (VIII-DK) had v_{ad}^* of 12.42 \pm 04.4 and 12.24 \pm 04.60 cm s^{-1} , respectively,

656 when measuring 15 m from the elevated source. During VII-CH and VIII-DK the temperature differed
 657 1°C and the relative humidity was approximately the same, but wind speed and solar radiation differed
 658 (Table 2 Supplementary information, Table S2). However, comparing the apparent deposition velocities
 659 from these experiments show comparable values for Lines 2 and 3, but higher values for Line 1. Overall,
 660 the Q/Q values for Line 1 were worse than MD and Lines 2 and 3, which is reflected in the higher
 661 apparent deposition velocities.



662

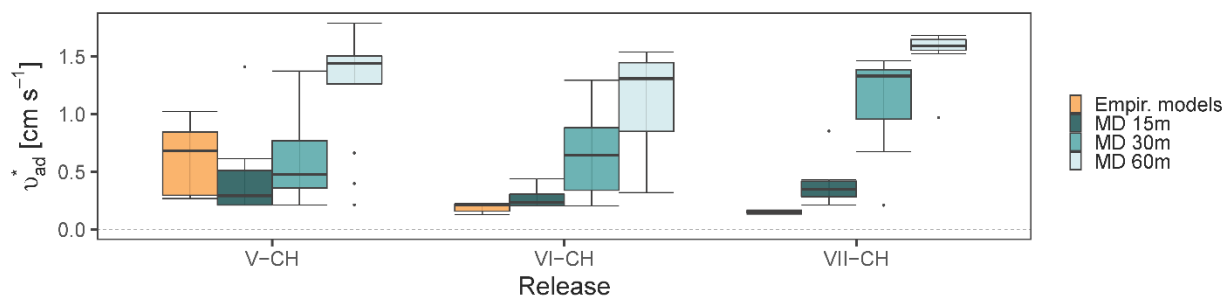


663

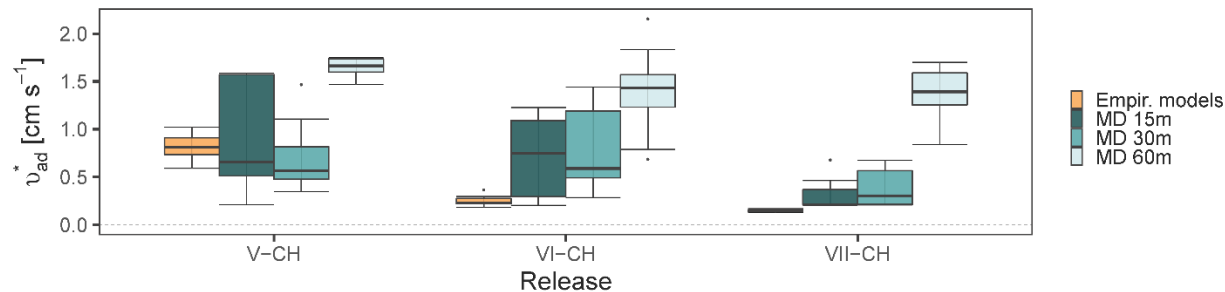
664 Figure 57.- Corresponding apparent surface deposition velocities (v_{ad}^*) required to have a recovery rate
 665 Q_{bLS}/Q closest to 1 in all the releases. The error bars represent the standard deviations. All values are
 666 shown in Table S1 in the Supplementary Information.

667 Many factors affect the deposition velocity, but it is possible to calculate v_{ad}^* from empirical
 668 models as explained previously (see section 2.6). Figure 6 Figure 8 shows v_{ad}^* for MDs in V-CH, VII-CH,
 669 and VIII-CH compared to v_{ad}^* calculated with the empirical models (equations 3-8). Using the empirical
 670 models, v_{ad}^* varies from 0.13 to 1.02 cm s^{-1} , increasing with the relative humidity (87%, 76% and 52%
 671 RH in V-CH, VI-CH and VII-CH, respectively). The difference between the two ways of estimating v_{ad}^*
 672 is not surprising since: i) bLS-derived deposition may be influenced by methodological uncertainties and

673 therefore deviate from true deposition, ii) calculated resistances are associated with uncertainties due to
 674 estimations of physical parameters. highlights the complexity and uncertainty for these methods. In
 675 addition, an artificial source most likely will have ~~has~~ higher v_{ad}^* than what is expected from a typical a-real
 676 agricultural source (Häni et al., 2018). This is expected because an artificial source with discrete outlets
 677 orifices located near the ground (with a high capacity for uptake) will have a larger deposition velocity
 678 close to the release because the ground has a high capacity for NH_3 sorption. On the contrary, a constantly
 679 and homogeneously (uniform) emitting source (e.g. storage tank or manure pile) is not expected to have
 680 any significant deposition within the source. -This is seen with the higher v_{ad}^* values found in these
 681 experiments compared to the calculated values with the empirical models. The height of the source might
 682 also have an influence on v_{ad}^* . This is indicated by the lowest v_{ad}^* in VII-CH, where the source was
 683 elevated compared to V-CH and VI-CH, where the gas was released on the surface. Placing the source
 684 above ground level will reduce the obstacles (crop on the field) for gas dispersion, reducing surface
 685 deposition. However, the bLS model does not consider the height of the source. For example, evaluating
 686 emissions from the application of liquid animal manure (ground level source) or a dairy housing (elevated
 687 source) will have different v_{ad}^* .



688



689

690 *Figure 68.- Corresponding apparent surface deposition velocities (v_{ad}^*) required to have a*
 691 *recovery rate Q_{bLS}/Q closest to 1 for miniDOAS (MD) in release V-CH, VI-CH and VII-CH and v_{ad}^**
 692 *calculated with an empirical models.*

693

694 3.5 Uncertainties and Sensitivity analysis

695 The line-integrated concentration measurement systems with a CRDS analyzer (Line 1, Line 2, and
 696 Line 3; excluding one value at 60 m) had an average recovery rate of CH₄ of 96%±4% (1 standard
 697 deviation, n =8)(not significantly different from 100%, see also Table xx2). Based on this, it is concluded
 698 that the method is not biased with respect to CH₄. The overall precision of CH₄ concentration
 699 measurements observed for the three versions of the line ranged from 4% to 22% at 15 m distance (see
 700 Table 2). However, the equivalent precision for NH₃ concentrations measurements was between 13%
 701 and 23% (Table 2) for the improved sampling lines (Line 2 and Line 3) at 15 m distance (CRE IV and
 702 CRE VIII). Comparing the 9% difference between the NH₃ recovery rates for from the MD at 15m (CRE
 703 V-CH – VII-CH) and for Line 2-3- and Line 3-at 15m distance, a 9% is assessed to represent the
 704 measurement bias-sampling line adsorption bias was related to the line-integrated system under the best
 705 conditions (improved sampling lines and moderate to warm temperatures). In addition, other factors
 706 related to the method affect the uncertainties on the determination of emission rates. The most relevant
 707 factors affecting the uncertainties are the precision determination of the wind direction
 708 measurement offset, canopy height and downwind concentration analyzer height, precision the
 709 Furthermore, the accuracy of the concentration analyzers measurements, and data filtering criteria of the
 710 bLS model related to the meteorological conditions (e.g., Flesch et al., 2005) are other important factors

711 that influence the uncertainty of the measurement. It would require a comprehensive study Since it is
712 quite a complex study to consider evaluate the contributions of ~~all these parameters~~, which is not the
713 scope of this study. Therefore, only a sensitivity e-analyseis of the wind direction offset and the sensor
714 height areis included below. The individual uncertainty contributions would be lumped into the overall
715 precision and bias mentioned above.

716 of the bLS model with respect to the precisions of wind directions and height of the analyzer was
717 investigated.

718 A sensitivity analysis of two input parameters for the bLS model was based on the resulting Q/Q
719 ratio when changing the inlet height of the analyzer and the wind direction offset compared to the valid
720 measured values in release VIII-DK. This was done for 11 fluxes in average intervals of 15 min, where all
721 emissions were estimated again with the bLS model. For the assessment of the influence of the input for
722 the measurement height all other variables were kept constant. Likewise, for the influence of the wind
723 direction, all other variables were kept constant while the wind direction offset was changed. The results
724 are presented in Figure S4 in the Supplementary Information, where it can be seen that Q/Q was most
725 sensitive to the changes in wind direction offset, stressing the importance of the true offset in wind
726 direction. Therefore, the wind direction must be thoroughly evaluated for the accuracy of emission
727 estimation since more or less trajectories have touchdowns inside of the source area for the dispersion
728 factor (Eq. 2). In addition, the uncertainty of Q/Q ratio increases as wind direction offset increases. The
729 emission estimation accuracy from point systems is more sensitive to error in the measured wind direction
730 (Flesch et al., 2004).

731 The accuracy and precision of the emission estimation also depends on the detection limits of the
732 concentration sensor analyzer, especially when the downwind concentration is close to the background
733 level, as it was shown previously (see section 3.2). Therefore, it is recommended to conduct concentration

734 and turbulence measurements not far from the source but minimum 10 times the source height according
735 to Harper et al. (2011) at a known height to reduce the uncertainty of the calculated emissions rates.

736 4 Conclusion

737 Line-average concentration measurement with a closed-path analyzer is comparable with an open-
738 path system, as the average of all releases with all instrument types, the CH₄ recovery rate Q_{bLS}/Q was
739 0.95 ± 0.08 ($n = 19$). Under comparable conditions, ~~an~~ average NH₃-recovery rates of 0.82 ± 0.05 ($n = 3$)
740 and 0.91 ± 0.07 ($n = 3$) for NH₃ and 0.94 ± 0.02 ($n = 3$) and 0.93 ± 0.05 ($n = 3$) for CH₄ were obtained
741 with the closed-path and open-path line integrated system, respectively. The implementation of the new
742 method presented in this study will enable measurement of fluxes of multiple gases from different type of
743 sources and evaluate the effects of mitigation strategies on emissions. In addition, this method allows for
744 continuous online measurements that resolve temporal variation in NH₃ emissions and the peak emissions
745 of CH₄. In addition, It is stressed that the wind direction must be thoroughly evaluated for the accuracy of
746 emission estimation with the bLS model.

747 A significant fraction of the emitted NH₃ is deposited near the source. Consequently, including the
748 deposition algorithm in the bLS model will have less bias a greater influence on the emission evaluation
749 at ground level sources (e.g. application of liquid animal manure), compared to elevated sources (e.g.
750 slurry tank). The present study shows that the estimated deposition velocities are in the same order of
751 magnitude in all the releases with some variation across the different approaches (instrument, distance,
752 method). ~~algorithm included in the bLS model estimates correct NH₃ emissions that considers surface~~
753 ~~deposition. In addition, the wind direction must be thoroughly evaluated for the accuracy of emission~~
754 ~~estimation with the bLS model.~~

755 Acknowledgments

756 This study was funded by the Ministry of the Environment and Food of Denmark as a service
757 agreement 2019-760-001136. Thanks to Simon Bowald for his great ideas and his help with designing

758 and building up the Line 3. Also thanks to technicians Martin Häberli-Wyss, Peter Storegård Nielsen,
759 Jens Kristian Kristensen, and Heidi Grønbaek for their invaluable help during the experimental part of the
760 study.

761 **References**

762 2016/2284/EU, n.d. Directive (EU) 2016/2284 of the European Parliament and of the Council of
763 14 December 2016 on the reduction of national emissions of certain atmospheric pollutants,
764 amending Directive 2003/35/EC and repealing Directive 2001/81/EC.

765 Aneja, V.P., Schlesinger, W.H., Erisman, J.W., 2009. Effects of Agriculture upon the Air Quality
766 and Climate: Research, Policy, and Regulations. *Environmental Science & Technology* 43,
767 4234–4240. <https://doi.org/10.1021/es8024403>

768 Asman, W.A.H., van Jaarsveld, H.A., 1991. A variable-resolution transport model applied for
769 NH_x in Europe. *Atmospheric Environment* 445–464. [https://doi.org/10.1016/0960-](https://doi.org/10.1016/0960-1686(92)90329-J)
770 [1686\(92\)90329-J](https://doi.org/10.1016/0960-1686(92)90329-J)

771 Bai, M., Loh, Z., Griffith, D.W.T., Turner, D., Eckard, R., Edis, R., Denmead, O.T., Bryant,
772 G.W., Paton-Walsh, C., Tonini, M., McGinn, S.M., Chen, D., 2022. Performance of open-path
773 lasers and Fourier transform infrared spectroscopic systems in agriculture emissions research.
774 *Atmos. Meas. Tech.* 15, 3593–3610. <https://doi.org/10.5194/amt-15-3593-2022>

775 Baldé, H., VanderZaag, A.C., Burt, S., Evans, L., Wagner-Riddle, C., Desjardins, R.L.,
776 MacDonald, J.D., 2016a. Measured versus modeled methane emissions from separated liquid
777 dairy manure show large model underestimates. *Agriculture, Ecosystems & Environment* 230,
778 261–270. <https://doi.org/10.1016/j.agee.2016.06.016>

779 Baldé, H., VanderZaag, A.C., Burt, S.D., Wagner-Riddle, C., Crolla, A., Desjardins, R.L.,
780 MacDonald, D.J., 2016b. Methane emissions from digestate at an agricultural biogas plant.
781 *Bioresource Technology* 216, 914–922. <https://doi.org/10.1016/j.biortech.2016.06.031>

782 Baldé, H., VanderZaag, A.C., Burt, S.D., Wagner-Riddle, C., Evans, L., Gordon, R., Desjardins,
783 R.L., MacDonald, J.D., 2018. Ammonia emissions from liquid manure storages are affected by
784 anaerobic digestion and solid-liquid separation. *Agricultural and Forest Meteorology* 258, 80–88.
785 <https://doi.org/10.1016/j.agrformet.2018.01.036>

786 Bühler, M., Häni, C., Ammann, C., Mohn, J., Neftel, A., Schrade, S., Zähler, M., Zeyer, K.,
787 Brönnimann, S., Kupper, T., 2021. Assessment of the inverse dispersion method for the
788 determination of methane emissions from a dairy housing. *Agricultural and Forest Meteorology*
789 307, 108501. <https://doi.org/10.1016/j.agrformet.2021.108501>

790 Carozzi, M., Loubet, B., Acutis, M., Rana, G., Ferrara, R.M., 2013. Inverse dispersion modelling
791 highlights the efficiency of slurry injection to reduce ammonia losses by agriculture in the Po
792 Valley (Italy). *Agricultural and Forest Meteorology* 171–172, 306–318.
793 <https://doi.org/10.1016/j.agrformet.2012.12.012>

794 Coates, T.W., Alam, M., Flesch, T.K., Hernandez-Ramirez, G., 2021. Field testing two flux
795 footprint models. *Atmos. Meas. Tech.* 14, 7147–7152. <https://doi.org/10.5194/amt-14-7147-2021>

796 DeBruyn, Z.J., Wagner-Riddle, C., VanderZaag, A., 2020. Assessment of Open-path
797 Spectrometer Accuracy at Low Path-integrated Methane Concentrations. *Atmosphere* 11, 184.
798 <https://doi.org/10.3390/atmos11020184>

799 Delre, A., Mønster, J., Samuelsson, J., Fredenslund, A.M., Scheutz, C., 2018. Emission
800 quantification using the tracer gas dispersion method: The influence of instrument, tracer gas
801 species and source simulation. *Science of The Total Environment* 634, 59–66.
802 <https://doi.org/10.1016/j.scitotenv.2018.03.289>

803 Desjardins, R.L., Denmead, O.T., Harper, L., McBain, M., Massé, D., Kaharabata, S., 2004.
804 Evaluation of a micrometeorological mass balance method employing an open-path laser for
805 measuring methane emissions. *Atmospheric Environment* 38, 6855–6866.
806 <https://doi.org/10.1016/j.atmosenv.2004.09.008>

807 EEA, 2019. EMEP/EEA air pollutant emission inventory guidebook 2019: technical guidance to
808 prepare national emission inventories. Publications Office, LU.

809 FAO, 2017. Food and Agriculture Organization of the United Nations. The future of food and
810 agriculture: trends and challenges. Food and Agriculture Organization of the United Nations,
811 Rome.

812 Flesch, T., Wilson, J., Harper, L., Crenna, B., 2005. Estimating gas emissions from a farm with
813 an inverse-dispersion technique. *Atmospheric Environment* 39, 4863–4874.
814 <https://doi.org/10.1016/j.atmosenv.2005.04.032>

815 Flesch, T.K., Desjardins, R.L., Worth, D., 2011. Fugitive methane emissions from an agricultural
816 biodigester. *Biomass and Bioenergy* 35, 3927–3935.
817 <https://doi.org/10.1016/j.biombioe.2011.06.009>

818 Flesch, T.K., McGinn, S.M., Chen, D., Wilson, J.D., Desjardins, R.L., 2014. Data filtering for
819 inverse dispersion emission calculations. *Agricultural and Forest Meteorology* 198–199, 1–6.
820 <https://doi.org/10.1016/j.agrformet.2014.07.010>

821 Flesch, T.K., Wilson, J.D., Harper, L.A., Crenna, B.P., Sharpe, R.R., 2004. Deducing Ground-to-
822 Air Emissions from Observed Trace Gas Concentrations: A Field Trial. *Journal of Applied*
823 *Meteorology* 43, 487–502. <https://doi.org/10.1175/JAM2214.1>

824 Flesch, T.K., Wilson, J.D., Harper, L.A., Todd, R.W., Cole, N.A., 2007. Determining ammonia
825 emissions from a cattle feedlot with an inverse dispersion technique. *Agricultural and Forest*
826 *Meteorology* 144, 139–155. <https://doi.org/10.1016/j.agrformet.2007.02.006>

827 Flesch, T.K., Wilson, J.D., Yee, E., 1995. Backward-Time Lagrangian Stochastic Dispersion
828 Model and Their Application to Estimate Gaseous Emissions. *Journal of Applied Meteorology*
829 34, 1320–1332. <https://doi.org/10.1175/1520-0450>

830 Fredenslund, A.M., Rees-White, T.C., Beaven, R.P., Delre, A., Finlayson, A., Helmore, J., Allen,
831 G., Scheutz, C., 2019. Validation and error assessment of the mobile tracer gas dispersion
832 method for measurement of fugitive emissions from area sources. *Waste Management* 83, 68–78.
833 <https://doi.org/10.1016/j.wasman.2018.10.036>

834 Gao, Z., Desjardins, R.L., Flesch, T.K., 2009. Comparison of a simplified micrometeorological
835 mass difference technique and an inverse dispersion technique for estimating methane emissions
836 from small area sources. *Agricultural and Forest Meteorology* 149, 891–898.
837 <https://doi.org/10.1016/j.agrformet.2008.11.005>

838 Gao, Z., Desjardins, R.L., van Haarlem, R.P., Flesch, T.K., 2008. Estimating Gas Emissions
839 from Multiple Sources Using a Backward Lagrangian Stochastic Model. *Journal of the Air &*
840 *Waste Management Association* 58, 1415–1421. <https://doi.org/10.3155/1047-3289.58.11.1415>

841 Garland, J.A., 1977. The dry deposition of sulphur dioxide to land and water surfaces. *Proc. R.*
842 *Soc. Lond. A* 354, 245–268. <https://doi.org/10.1098/rspa.1977.0066>

843 Grant, R.H., Boehm, M.T., Bogan, B.W., 2015. Methane and carbon dioxide emissions from
844 manure storage facilities at two free-stall dairies. *Agricultural and Forest Meteorology* 213, 102–
845 113. <https://doi.org/10.1016/j.agrformet.2015.06.008>

846 Hafner, S.D., 2018. The ALFAM2 database on ammonia emission from field-applied manure_
847 Description and illustrative analysis. *Agricultural and Forest Meteorology* 14.

848 Häni, C., Bühler, M., Neftel, A., Ammann, C., Kupper, T., 2021. Performance of open-path
849 GasFinder3 devices for CH₄ concentration measurements close to ambient levels. *Atmos. Meas.*
850 *Tech.* 14, 1733–1741. <https://doi.org/10.5194/amt-14-1733-2021>

851 Häni, C., Flechard, C., Neftel, A., Sintermann, J., Kupper, T., 2018. Accounting for Field-Scale
852 Dry Deposition in Backward Lagrangian Stochastic Dispersion Modelling of NH₃ Emissions.
853 <https://doi.org/10.20944/preprints201803.0026.v1>

854 Harper, L.A., Denmead, O.T., Flesch, T.K., 2011. Micrometeorological techniques for
855 measurement of enteric greenhouse gas emissions. *Animal Feed Science and Technology* 166–
856 167, 227–239. <https://doi.org/10.1016/j.anifeedsci.2011.04.013>

857 Harper, L.A., Flesch, T.K., Powell, J.M., Coblenz, W.K., Jokela, W.E., Martin, N.P., 2009.
858 Ammonia emissions from dairy production in Wisconsin. *Journal of Dairy Science* 92, 2326–
859 2337. <https://doi.org/10.3168/jds.2008-1753>

860 Harper, L.A., Flesch, T.K., Weaver, K.H., Wilson, J.D., 2010. The Effect of Biofuel Production
861 on Swine Farm Methane and Ammonia Emissions. *Environmental Quality* 39, 1984–1992.
862 <https://doi.org/10.2134/jeq2010.0172>

863 Hicks, B.B., Baldocchi, D.D., Meyers, T.P., Hosker, R.P., Matt, D.R., 1987. A preliminary
864 multiple resistance routine for deriving dry deposition velocities from measured quantities.
865 *Water Air Soil Pollut* 36, 311–330. <https://doi.org/10.1007/BF00229675>

866 Hu, E., Babcock, E.L., Bialkowski, S.E., Jones, S.B., Tuller, M., 2014. Methods and Techniques
867 for Measuring Gas Emissions from Agricultural and Animal Feeding Operations. *Critical*
868 *Reviews in Analytical Chemistry* 44, 200–219. <https://doi.org/10.1080/10408347.2013.843055>

869 Hu, N., Flesch, T.K., Wilson, J.D., Baron, V.S., Basarab, J.A., 2016. Refining an inverse
870 dispersion method to quantify gas sources on rolling terrain. *Agricultural and Forest*
871 *Meteorology* 225, 1–7. <https://doi.org/10.1016/j.agrformet.2016.05.007>

872 Kamp, J.N., Chowdhury, A., Adamsen, A.P.S., Feilberg, A., 2019. Negligible influence of
873 livestock contaminants and sampling system on ammonia measurements with cavity ring-down
874 spectroscopy. *Measurement Techniques* 12, 2837–2850. [https://doi.org/10.5194/amt-12-2837-](https://doi.org/10.5194/amt-12-2837-2019)
875 2019

876 Kamp, J.N., Häni, C., Nyord, T., Feilberg, A., Sørensen, L.L., 2021. Calculation of NH₃
877 Emissions, Evaluation of Backward Lagrangian Stochastic Dispersion Model and Aerodynamic
878 Gradient Method 17.

879 Kupper, T., Eugster, R., Sintermann, J., Häni, C., 2021. Ammonia emissions from an uncovered
880 dairy slurry storage tank over two years: Interactions with tank operations and meteorological
881 conditions. *Biosystems Engineering* 204, 36–49.
882 <https://doi.org/10.1016/j.biosystemseng.2021.01.001>

883 Lemes, Y.M., Garcia, P., Nyord, T., Feilberg, A., Kamp, J.N., 2022. Full-scale investigation of
884 methane and ammonia mitigation by early single-dose slurry storage acidification [Submitted
885 June 2022].

886 Lynn, B.H., Carlson, T.N., 1990. A stomatal resistance model illustrating plant vs. external
887 control of transpiration. *Agricultural and Forest Meteorology* 52, 5–43.
888 [https://doi.org/10.1016/0168-1923\(90\)90099-R](https://doi.org/10.1016/0168-1923(90)90099-R)

889 Massad, R.-S., Nemitz, E., Sutton, M.A., 2010. Review and parameterisation of bi-directional
890 ammonia exchange between vegetation and the atmosphere. *Atmos. Chem. Phys.* 10, 10359–
891 10386. <https://doi.org/10.5194/acp-10-10359-2010>

892 McBain, M.C., Desjardins, R.L., 2005a. The evaluation of a backward Lagrangian stochastic
893 (bLS) model to estimate greenhouse gas emissions from agricultural sources using a synthetic
894 tracer source. *Agricultural and Forest Meteorology* 135, 61–72.
895 <https://doi.org/10.1016/j.agrformet.2005.10.003>

896 McBain, M.C., Desjardins, R.L., 2005b. The evaluation of a backward Lagrangian stochastic
897 (bLS) model to estimate greenhouse gas emissions from agricultural sources using a synthetic
898 tracer source. *Agricultural and Forest Meteorology* 135, 61–72.
899 <https://doi.org/10.1016/j.agrformet.2005.10.003>

900 McGinn, S.M., Coates, T., Flesch, T.K., Crenna, B., 2008. Ammonia emission from dairy cow
901 manure stored in a lagoon over summer. *Can. J. Soil. Sci.* 88, 611–615.
902 <https://doi.org/10.4141/CJSS08002>

903 McGinn, S.M., Flesch, T.K., Beauchemin, K.A., Shreck, A., Kindermann, M., 2019.
904 *Micrometeorological Methods for Measuring Methane Emission Reduction at Beef Cattle*
905 *Feedlots: Evaluation of 3-Nitrooxypropanol Feed Additive. J. environ. qual.* 48, 1454–1461.
906 <https://doi.org/10.2134/jeq2018.11.0412>

907 McGinn, S.M., Flesch, T.K., Crenna, B.P., Beauchemin, K.A., Coates, T., 2007. Quantifying
908 Ammonia Emissions from a Cattle Feedlot using a Dispersion Model. *J. Environ. Qual.* 36,
909 1585–1590. <https://doi.org/10.2134/jeq2007.0167>

910 McGinn, S.M., Turner, D., Tomkins, N., Charmley, E., Bishop-Hurley, G., Chen, D., 2011.
911 *Methane Emissions from Grazing Cattle Using Point-Source Dispersion. J. Environ. Qual.* 40,
912 22–27. <https://doi.org/10.2134/jeq2010.0239>

913 OECD, FAO, 2019. *OECD-FAO Agricultural Outlook 2019-2028, OECD-FAO Agricultural*
914 *Outlook. OECD.* https://doi.org/10.1787/agr_outlook-2019-en

915 Pedersen, J.M., Feilberg, A., Kamp, J.N., Hafner, S., Nyord, T., 2020. Ammonia emission
916 measurement with an online wind tunnel system for evaluation of manure application techniques.
917 Atmospheric Environment 230, 117562. <https://doi.org/10.1016/j.atmosenv.2020.117562>

918 Platt, U., Stutz, J., 2008. Differential optical absorption spectroscopy: principles and
919 applications, Physics of Earth and space environments. Springer, Berlin.

920 R Core Team, 2018. R: A language and environment for statistical computing; R Foundation for
921 Statistical. Computing: Vienna, Austria.

922 Ro, K.S., Johnson, M.H., Hunt, P.G., Flesch, T.K., 2011. Measuring Trace Gas Emission from
923 Multi-Distributed Sources Using Vertical Radial Plume Mapping (VRPM) and Backward
924 Lagrangian Stochastic (bLS) Techniques. Atmosphere 2, 553–566.
925 <https://doi.org/10.3390/atmos2030553>

926 Ro, K.S., Stone, K.C., Johnson, M.H., Hunt, P.G., Flesch, T.K., Todd, R.W., 2014. Optimal
927 Sensor Locations for the Backward Lagrangian Stochastic Technique in Measuring Lagoon Gas
928 Emission. Journal of Environmental Quality 43, 1111–1118.
929 <https://doi.org/10.2134/jeq2013.05.0163>

930 Sanz, A., Misselbrook, T., Sanz, M.J., Vallejo, A., 2010. Use of an inverse dispersion technique
931 for estimating ammonia emission from surface-applied slurry. Atmospheric Environment 44,
932 999–1002. <https://doi.org/10.1016/j.atmosenv.2009.08.044>

933 Shah, S.B., Grabow, G.L., Westerman, P.W., 2006. Ammonia Adsorption in Five Types of
934 Flexible Tubing Materials. Applied Engineering in Agriculture 22, 919–923.
935 <https://doi.org/10.13031/2013.22253>

936 Sintermann, J., Ammann, C., Kuhn, U., Spirig, C., Hirschberger, R., Gärtner, A., Neftel, A.,
937 2011. Determination of field scale ammonia emissions for common slurry spreading practice
938 with two independent methods. *Atmospheric Measurement Techniques* 4, 1821–1840.
939 <https://doi.org/10.5194/amt-4-1821-2011>

940 Sintermann, J., Dietrich, K., Häni, C., Bell, M., Jocher, M., Neftel, A., 2016. A miniDOAS
941 instrument optimised for ammonia field measurements. *Atmospheric Measurement Techniques*
942 9, 2721–2734. <https://doi.org/10.5194/amt-9-2721-2016>

943 Sommer, S.G., McGinn, S.M., Hao, X., Larney, F.J., 2004. Techniques for measuring gas
944 emissions from a composting stockpile of cattle manure. *Atmospheric Environment* 38, 4643–
945 4652. <https://doi.org/10.1016/j.atmosenv.2004.05.014>

946 Todd, R.W., Cole, N.A., Rhoades, M.B., Parker, D.B., Casey, K.D., 2011. Daily, Monthly,
947 Seasonal, and Annual Ammonia Emissions from Southern High Plains Cattle Feedyards. *J.*
948 *Environ. Qual.* 40, 1090–1095. <https://doi.org/10.2134/jeq2010.0307>

949 Vaittinen, O., Metsälä, M., Persijn, S., Vainio, M., Halonen, L., 2014. Adsorption of ammonia on
950 treated stainless steel and polymer surfaces. *Applied Physics B* 115, 185–196.
951 <https://doi.org/10.1007/s00340-013-5590-3>

952 van Haarlem, R.P., Desjardins, R.L., Gao, Z., Flesch, T.K., Li, X., 2008. Methane and ammonia
953 emissions from a beef feedlot in western Canada for a twelve-day period in the fall. *Can. J.*
954 *Anim. Sci.* 88, 641–649. <https://doi.org/10.4141/CJAS08034>

955 VanderZaag, A.C., Flesch, T.K., Desjardins, R.L., Baldé, H., Wright, T., 2014. Measuring
956 methane emissions from two dairy farms: Seasonal and manure-management effects.

957 Agricultural and Forest Meteorology 194, 259–267.
958 <https://doi.org/10.1016/j.agrformet.2014.02.003>

959 Vechi, N.T., Mellqvist, J., Scheutz, C., 2022. Quantification of methane emissions from cattle
960 farms, using the tracer gas dispersion method. Agriculture, Ecosystems & Environment 330,
961 107885. <https://doi.org/10.1016/j.agee.2022.107885>

962 Voglmeier, K., Jocher, M., Häni, C., Ammann, C., 2018. Ammonia emission measurements of
963 an intensively grazed pasture. Biogeosciences 15, 4593–4608. [https://doi.org/10.5194/bg-15-](https://doi.org/10.5194/bg-15-4593-2018)
964 4593-2018

965 Wesely, M., 2007. Parameterization of surface resistances to gaseous dry deposition in regional-
966 scale numerical models☆. Atmospheric Environment 41, 52–63.
967 <https://doi.org/10.1016/j.atmosenv.2007.10.058>

968 Wilson, J.D., Flesch, T.K., Harper, L.A., 2001. Micro-meteorological methods for estimating
969 surface exchange with a disturbed windflow. Agricultural and Forest Meteorology 107, 207–225.
970 [https://doi.org/10.1016/S0168-1923\(00\)00238-0](https://doi.org/10.1016/S0168-1923(00)00238-0)

971 Yang, W., Que, H., Wang, S., Zhu, A., Zhang, Y., He, Y., Xin, X., Zhang, X., 2019. Comparison
972 of backward Lagrangian stochastic model with micrometeorological mass balance method for
973 measuring ammonia emissions from rice field. Atmospheric Environment 211, 268–273.
974 <https://doi.org/10.1016/j.atmosenv.2019.05.028>

975